

# Synthesis of MgO-ZrO<sub>2</sub> Mixed Nanoparticles via Different Precursors: Identification of their Destructive Action for Organic Pollutants

Islam MI Moustafa\* and Mohamed R Abdelhamid

Department of Chemistry, Faculty of Science, Benha University, 13518, Egypt

\*Corresponding author: Islam MI Moustafa, Department of Chemistry, Faculty of Science, Benha University, 13518, Egypt, Tel: +201333222578; E-mail: islamshahin84@outlook.com

Received date: November 18, 2017; Accepted date: January 17, 2017; Published date: February 02, 2017

Copyright: © 2018 Moustafa IMI, et al. This is an open-access article distributed under the terms of the Creative Commons Attribution License, which permits unrestricted use, distribution, and reproduction in any medium, provided the original author and source are credited.

## Abstract

Nanocrystalline mixed Magnesium-Zirconyl oxides were prepared by co-precipitation method starting from different organic acid precursors and glycine. The as-prepared nanooxides were characterized by X-Ray Diffraction, TGA-DTA, HR-TEM, electronic absorption spectra and FTIR spectroscopic techniques. The results confirmed the formation of mixed MgO-ZrO<sub>2</sub> (cubic, orthorhombic) nanooxides with crystallite size ranging from 10.79-47.55 nm depending on the organic precursors used. The UV-Vis spectroscopy showed the semiconductor nature of the samples with optical energy gap ranging from 2.85-3.00 eV. The morphology and microstructure characteristics were also obtained by High Resolution Transmission Electron Microscopy (HRTEM). The products had been tested as destructive adsorbents for the decontamination of Malathion as VX Chemical Warfare Agent (CWA) stimulant, where it was found that complete decontamination took place within 240 min. The photoactivity of the prepared samples was assessed by the photocatalytic decomposition of Orange G dye in an aqueous solution under irradiation of UV radiation of 365 nm wavelength.

**Keywords:** Nano sized MgO-ZrO<sub>2</sub> mixed oxides; Decontamination; VX stimulant; Orange G

## Abbreviations:

CWA: Chemical Warfare Agent; OG: Orange G.

## Introduction

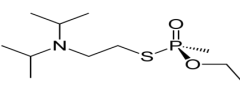
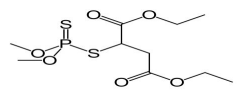
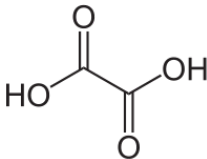
Nanomaterials are considered as next generation materials that have attracted recent attention due to their novel properties differing from those of the bulk materials. Nanooxides play an important role in applied chemistry due to their vast applications such as semiconductors [1], biodiesel applications [2], catalytic application [3,4], biological applications [5], glaze applications [6], purification of oils [7] and photocatalytic degradation of organic pollutants [8-12]. Though many sorbents were tried for the decontamination of CWA's; viz activated carbon [13,14] or polymer [15,16], but the use of mixed metal oxide nanoparticles showed more satisfactory results [17,18] due to their high surface area, crystallinity, different morphologies and easily separation of electron hole pairs which are necessary for generating free radicals which decompose these organic pollutants [19]. Among of these oxides, very little work about the nanoscaled Magnesia-Zirconia mixed oxides (MgO-ZrO<sub>2</sub>) was reported throughout literature survey. So, in continuity to our previous work [20] on the preparation of simple ZrO<sub>2</sub> nanoparticles from different organic acid precursors, it was found quit fruitful to study the effect of starting organic acid and glycine precursors on the crystal size and morphology of mixed MgO-ZrO<sub>2</sub> nanooxides. The prepared nanoparticles were found to be excellent adsorbents for the decontamination of Malathion as stimulant of VX CWA and OG as organic pollutant.

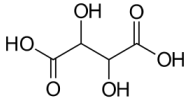
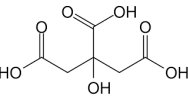
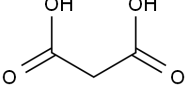
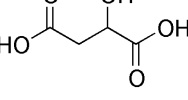
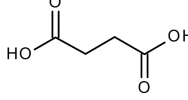
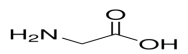
## Materials and Methods

### Chemicals

All chemicals used in the present work were of the highest purity available and were used without any purification. Freshly bidistilled water and spec pure solvents were used whenever is necessary.

For studying the most famous nerve agent, Malathion was used as the stimulant of VX {O-ethyl-S-(2-diisopropylaminoethyl)-methylphosphono-thiolate}. Malathion and OG were obtained from Merck chemical company and were used as received. Table 1 demonstrates the structures of Malathion, VX and the organic acids used as precursors.

Nerve agent	Stimulant
VX 	Malathion 
Organic acid	Structure
Oxalic acid	

Tartaric acid	
Citric acid	
Malonic acid	
Malic acid	
Succinic acid	
Glycine	

**Table 1:** Structures of Malathion, VX, organic acids and Glycine used as precursors.

### Synthesis of mixed MgO-ZrO<sub>2</sub> nanoparticles

Mixed Magnesium-Zirconyl oxides nanoparticles (MZ1-MZ7) were prepared via co-precipitation of 50 ml of each of 0.1 M ZrO<sub>2</sub>Cl<sub>2</sub>·8H<sub>2</sub>O: 0.1 M Mg(CH<sub>3</sub>COO)<sub>2</sub>·4H<sub>2</sub>O:0.2 M different organic acids viz: Oxalic (MZ1), Tartaric (MZ2), Citric (MZ3), Malonic (MZ4), Malic (MZ5), Succinic (MZ6) and Glycine (MZ7). The mixtures were stirred for 1 h, heated for another 1 h and the precipitates so formed were filtered and washed thoroughly with bidistilled water. The dried precipitates were finely ignited at 750°C for 5 h to get the corresponding final mixed nanooxides.

### Physical measurements

All physical measurements were carried out using the same instruments and under the same conditions described in our previous work [20]. FTIR spectra (Nicolet iSio FTIR spectrophotometer), Electronic absorption spectra (Jasco V-530 UV-Vis spectrophotometer), Thermogravimetric analyses (Shimadzu TA-60 WS thermal analysis), X-Ray powder diffraction spectra (on 18 KW diffractometer Bruker). Model D8 Advance with monochromator Cu, K $\alpha$  radiation;  $\lambda$ =1.54178 Å, and HR-TEM (JOEL; model 1200 EX with an accelerator voltage of 220 kV).

### Method of CWA disintegrations

Synthesized powdery samples were dried over 24 hours in a vacuum kiln (at 100°C) before tests. Weighed portion of the given nanosized sample was put into a glass vial provided with a screw solid cap. The toxic agent was dosed onto the powder reagent layer in the form of a solution in acetone solvent. The vial was sealed with a cap and put into

a thermostat (25°C). Suspension was vigorously agitated and liquid fraction was separated from the solid using a centrifuge. Adding of Isopropyl alcohol (2 ml) terminated the reaction, sequent the electronic absorption spectra were measured for the residual content of Malathion. The respective detoxification capabilities of the evaluated samples were expressed as percentages of Malathion elimination from the reaction mixture under the given experimental conditions.

### Photocatalytic activity for OG

For a typical photocatalytic degradation of OG dye in aqueous solution, 100 mg of sample was added to 100 ml of 20 ppm aqueous dye solution which was kept in dark for 6 h to reach an adsorption desorption equilibrium, then 0.5 M H<sub>2</sub>O<sub>2</sub> solution was added. The degradation process was operated under UV irradiation using a 250 W Xenon arc lamp (Toshiba, SHLS-002;  $\lambda$ =365 nm). After different time intervals, the catalyst was recovered by centrifugation and the absorbance of the clear solution was measured at 485 nm ( $\lambda_{\text{max}}$  for OG).

## Results and Discussion

### Thermal analysis

Inspection of thermal analysis of the precursors (representative examples of MZ2 and MZ3 are shown in Figure 1, while thermal data are summarized in Table 2) shows that they thermally degraded through three main steps. The first, within the temperature range 86-190°C, is due to the removal of humidity and water of crystallization. The second and third steps at the temperature ranges 229.5-433.32°C and 336.0-617.7°C are due to the thermal decomposition of Magnesium and Zirconium precursors, respectively. These steps led to the formation of mixed nanooxides MgO-ZrO<sub>2</sub> as final products.

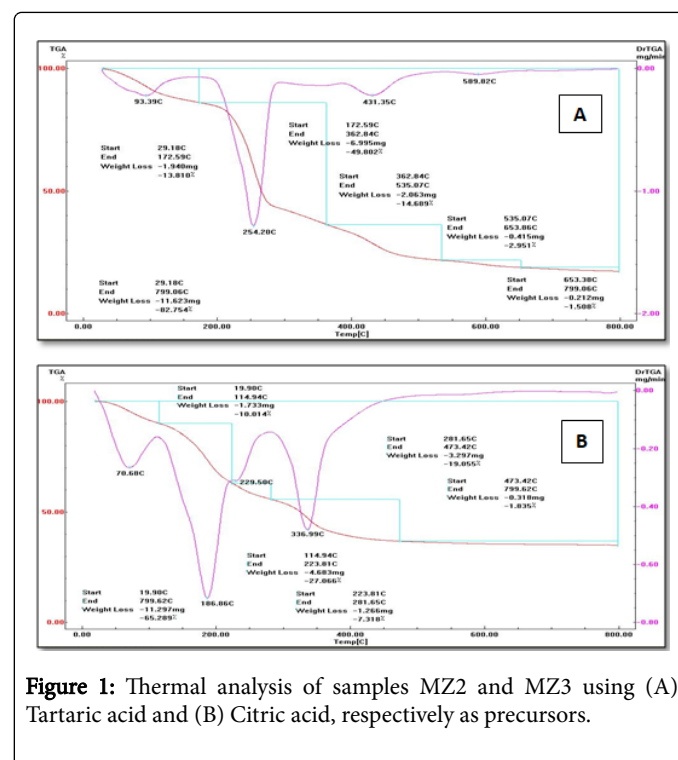


**Figure 1:** Thermal analysis of samples MZ2 and MZ3 using (A) Tartaric acid and (B) Citric acid, respectively as precursors.

Compound	Temp. (°C)	Weight loss %	Assignment
MZ1	190.75	21.17	Removal of water of crystallization
	410.27	28.85	Decomposition of Magnesium oxalate
	484.02	17.13	Decomposition of Zirconium oxalate
MZ2	93.39	13.81	Removal of water of crystallization
	254.2	49.8	Decomposition of Magnesium tartrate
	431.35	17.64	Decomposition of Zirconium tartrate
MZ3	86.08	10.22	Removal of water of crystallization
	322.46	13.1	Decomposition of Magnesium citrate
	522.49	11.35	Decomposition of Zirconium citrate
MZ4	186.86	27.07	Removal of water of crystallization
	229.5	17.33	Decomposition of Magnesium malonate
	336	19.06	Decomposition of Zirconium malonate
MZ5	171.46	16.22	Removal of water of crystallization
	386.47	16.94	Decomposition of Magnesium malate
	497.82	21.12	Decomposition of Zirconium malate
MZ6	182.83	8.84	Removal of water of crystallization
	397.82	20.7	Decomposition of Magnesium succinate
	486.82	12.82	Decomposition of Zirconium succinate
MZ7	102.38	22.78	Removal of water of crystallization
	433.32	11.33	Decomposition of Magnesium salt of Glycine
	617.07	34.8	Decomposition of Zirconium salt of Glycine

**Table 2:** Thermogravimetric data for different organic precursors.

### FTIR spectra

The Fourier Transform Infrared spectra (FTIR) of both the organic acid and Glycine precursors before ignition and those of the

nanoparticles calcined at 750°C were studied. The spectra of the formers show characteristic band frequencies of the functional groups  $\nu_{OH}$ ,  $\nu_{NH_2}$  (for Glycine),  $\nu_{C=O}$ ,  $\nu_{Zr-O}$ ,  $\nu_{Mg-O}$  and  $\delta_{OH}$  as shown in Table 3. On the other hand, the spectra of the ignited samples showed the disappearance of the band frequencies of the functional groups of the organic precursors with the appearance of expected characteristic absorption bands in the short wavenumber region around 500 cm<sup>-1</sup> due to metal-oxygen stretching frequencies. The IR bands within the ranges 531.2-594.6 cm<sup>-1</sup> and 406.0-486.4 cm<sup>-1</sup> are due to the Zr-O and Mg-O in orthorhombic and cubic environment, respectively [21].

Sample	Precursor	IR frequency cm <sup>-1</sup>					
		$\nu_{OH}$	$\nu_{NH_2}$	$\nu_{C=O}$	$\delta_{OH}$	$\nu_{Zr-O}$	$\nu_{Mg-O}$
MZ1	Oxalic acid	3404.8	-	1674.8	911.2	531.7	484.6
MZ2	Tartaric	3410	-	1743	1094	549.4	485.1
MZ3	Citric acid	3384.5	-	1675	1018	5510	406
MZ4	Malonic acid	3381.4	-	1701.1	1031.4	594.6	486.4
MZ5	Malic acid	3374.7	-	1713.5	1015.4	542.5	420.4
MZ6	Succinic acid	3400.9	-	1693	1021	582.8	457.2
MZ7	Glycine	3404.6	3245	1636.4	1010	573.4	432.1

**Table 3:** IR frequencies (cm<sup>-1</sup>) of some important bands of the organic precursors.

### X-Ray Diffraction (XRD) studies

The purity and crystallinity of the obtained mixed MgO-ZrO<sub>2</sub> nanoparticles were examined by using powder XRD analysis. Figure 2 shows the XRD patterns of the mixed oxides prepared from different precursors and calcined at 750°C. The narrow line widths indicate a high crystallinity of the materials. ZrO<sub>2</sub> indexed orthorhombic phase of Zirconium oxide (JCPDS Card No. 01-079-1796) while MgO indexed cubic phase (JCPDS Card No. 01-071-1176). The mean crystallite sizes of the nanocrystalline materials estimated by using Scherrer formula [22] were found to depend on the starting organic precursors and lie in the range 10.79-47.55 nm (Table 4) with increasing size in the order: Glycine<Tartaric acid<Oxalic acid<Malic acid<Citric acid<Malonic acid<Succinic acid.

Sample	Precursor	XRD crystal size	Phase produced by XRD	Card No.	Crystal system
MZ1	Oxalic acid	19.53	Periclase-MgO	01-071-1176	Cubic
			Zirconium Oxide-ZrO <sub>2</sub>	01-079-1796	Orthorhombic
MZ2	Tartaric acid	15.6	Periclase-MgO	01-071-1176	Cubic
			Zirconium Oxide-ZrO <sub>2</sub>	01-079-1796	Orthorhombic
MZ3	Citric acid	28.24	Periclase-MgO	01-071-1176	Cubic
			Zirconium Oxide-ZrO <sub>2</sub>	01-079-1796	Orthorhombic
MZ4	Malonic acid	35.25	Periclase-MgO	01-071-1176	Cubic
			Zirconium Oxide-ZrO <sub>2</sub>	01-079-1796	Orthorhombic

MZ5	Malic acid	22.2	Periclase-MgO	01-071-1176	Cubic
			Zirconium Oxide-ZrO <sub>2</sub>	01-079-1796	Orthorhombic
			Zirconium Oxide-ZrO <sub>2</sub>	01-078-1807	Monoclinic
MZ6	Succinic acid	47.55	Periclase-MgO	01-071-1176	Cubic
			Zirconium Oxide-ZrO <sub>2</sub>	01-079-1796	Orthorhombic
MZ7	Glycine	10.79	Periclase-MgO	01-071-1176	Cubic
			Zirconium Oxide-ZrO <sub>2</sub>	01-079-1796	Orthorhombic

**Table 4:** Effect of organic acid precursors on the crystal size and morphology of the prepared nanooxides.

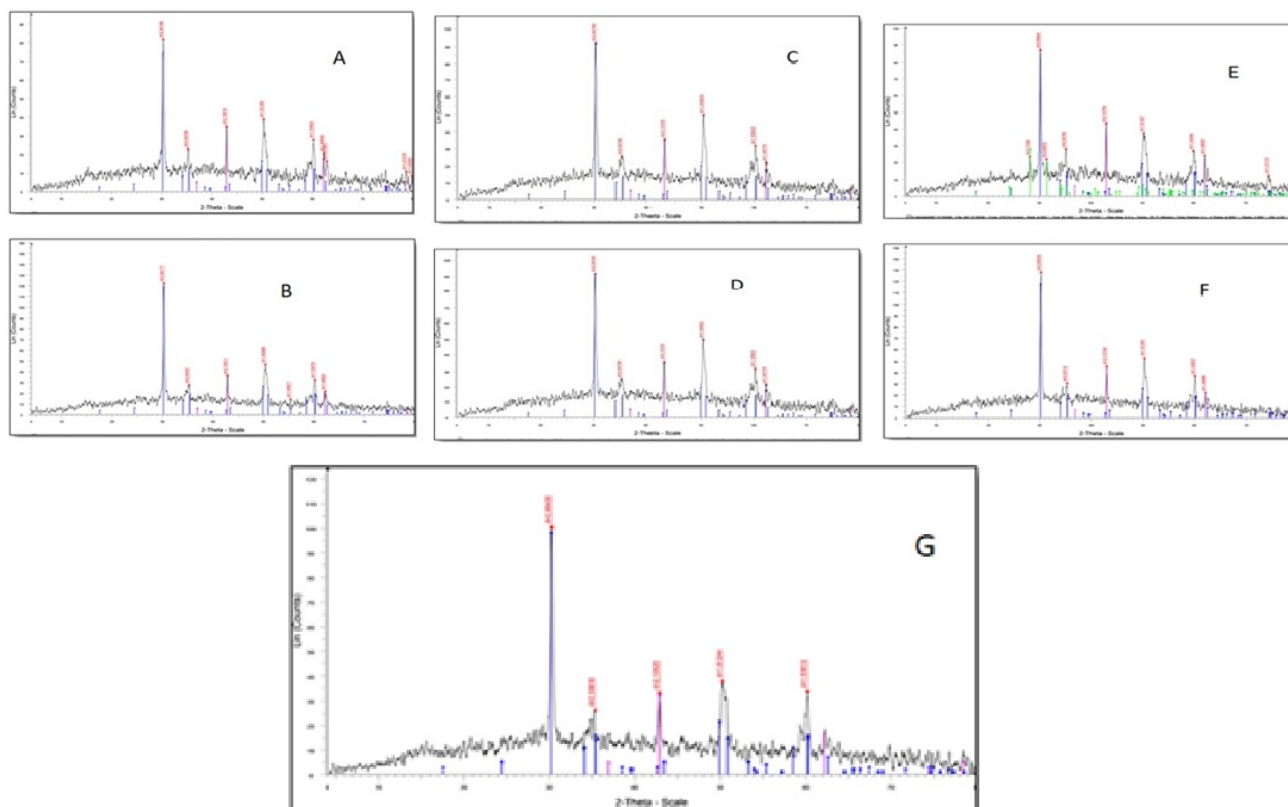


**Figure 2:** XRD of samples MZ1-MZ7 prepared using (A) Oxalic acid, (B) Tartaric acid, (C) Citric acid, (D) Malonic acid, (E) Malic acid, (F) Glycine and (G) Succinic acid.

## HR-TEM studies

The morphology and microstructure of some selected samples of the as-prepared nanooxides were studied using HR-TEM (Figure 3). The images reveal the cubical structure of samples MZ7 and MZ2 with average size of 8.31 and 12.45 nm, respectively, cylindrical shape with average crystal size of 26.43 nm for sample MZ3 and rectangular shape with average crystal size 20.8 nm for sample MZ4.

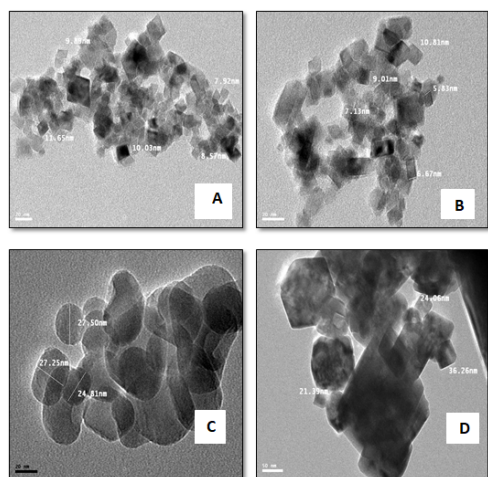


**Figure 3:** HR-TEM images for samples (A) MZ7, (B) MZ2, (C) MZ3 and (D) MZ4.

### Optical properties

The optical energy gaps of the prepared nanooxides were determined from the UV-Vis spectra in solid state (Nujol mull technique). The optical energy gaps ( $E_g$ ) can be calculated using the following equation:

$$(\alpha h\nu)^n = k(h\nu - E_g)$$

Where,  $\alpha$ =absorption coefficient,  $K$ =constant,  $E_g$ =band gap and  $n$ =an integer equals either 2 for a direct allowed transition or 1/2 for an indirect allowed transition.

For the prepared mixed oxide nanoparticles, direct allowed transitions are the predominant and hence  $(\alpha h\nu)^2$  are plotted versus  $h\nu$ , as shown in Figure 4. The optical energy gap ( $E_g$ ) for each nanoparticle is obtained from extrapolation of the graph to  $(\alpha h\nu)^2=0$ . The values of  $E_g$  (2.85, 2.97, 2.88, 3.00, 2.87, 3.00 and 2.95 eV) for the nanooxides MZ1 to MZ7, respectively proved that the prepared mixed oxides nanoparticles are semiconductors and are in an excellent agreement with the reported data [20].

### Decomposition of CWA on metal oxides

The photodegradation of Malathion as VX CWA stimulant was studied without using catalyst and with using sample MZ7 nanooxide (prepared from Glycine) as catalyst. The process was followed up by scanning the UV-Vis spectra within the range 220-350 nm (Figures 5 and 6) and the band of maximum absorbance at 238 nm was taken to follow up the degradation process. Inspection of the absorption spectra and the calculated % degradation values shows that, after 240 min Malathion degraded maximally up to 36.5% under the effect of UV radiation only, while the percent degradation efficiency reaches 91.13% on using sample MZ7 nanoparticle as catalyst within the same time interval.

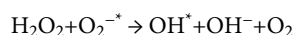
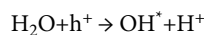
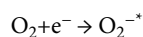
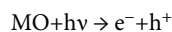
Metal oxides demonstrate superior ability to adsorb and decompose CWA compared to pure metal surfaces. This is often attributed to reactive sites on the metal oxide surface through which organophosphonate species (nerve agents) can adsorb and

subsequently undergo a hydrolysis reaction. It was found by Wagner [23], that each metal oxide hydrolyzed the CWA, resulting in surface-bound phosphonate products, as shown in Scheme 1. Wagner also found that the decomposition of the CWA, VX and GD over the MgO oxide nanoparticles showed that the phosphonate products were bound to the oxide surface and that the hydrolysis of VX did not lead to the formation of the toxic EA-2192 product.

### Photocatalytic activity of mixed oxide nanoparticles

Selected mixed oxide nanoparticle (sample MZ2; prepared from Tartaric acid as organic precursor) was tested as catalyst for the photocatalytic degradation of OG as model. 100 ml solution containing the OG dye (20 ppm) and the nanoparticle oxide (100 mg) was photo irradiated by UV light at different conditions, namely; (UV only), (UV+MZ2 only) and (UV+H<sub>2</sub>O<sub>2</sub>+MZ2). The degradation of the dye was followed up by recording the absorption spectra at different time intervals as shown graphically in Figures 7 and 8. The results showed that the maximum percent degradation of OG dye was 19.01% after 180 min in case of UV irradiation only (Figure 7) while almost 100.00% of the dye was decomposed under UV illumination in the presence of Hydrogen peroxide and MZ2 catalyst within 180 min (Figure 8) indicating the very high efficiency of the nanooxides (represented by sample MZ2) compared with others cited in literature [24].

The mechanism of photodegradation process in the presence of UV radiation and mixed oxide MgO-ZrO<sub>2</sub> is represented graphically in Figure 9. Upon absorption of photons with energies larger than the band gap of the mixed nanooxide, electrons are excited from the valence band to the conduction band, creating an electron hole  $h^+$ . These photogenerated charge carriers may undergo recombination, become trapped in metastable states, or migrate to the surface of the metal oxide, where they can react with adsorbed molecules. In an air-saturated aqueous environment, the photogenerated electrons and holes participate in reacting with dissolved molecular oxygen, surface hydroxyl groups, and adsorbed water molecules to form hydroxyl and superoxide radicals. Although the detailed mechanism of nanosized metal oxide photocatalysis reactions differs from one pollutant to another, but it has been widely recognized that superoxide and, specifically,  $\bullet OH$  hydroxyl radicals act as active reagents in the degradation of organic compounds. These radicals are formed by scavenging of the electron hole pair by molecular oxygen and water, through the following sequences:





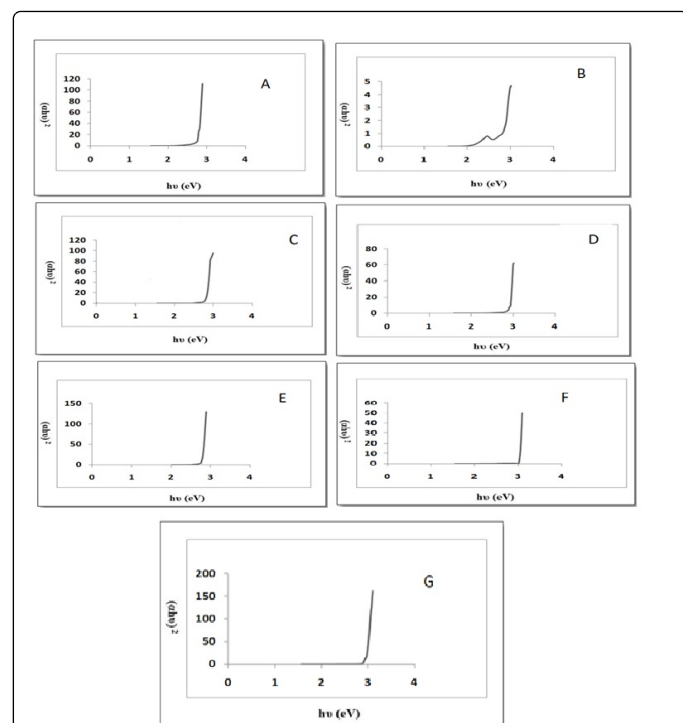


**Figure 4:** Optical energy gap of the samples MZ1-MZ7 using (A) Oxalic acid, (B) Tartaric acid, (C) Citric acid, (D) Malonic acid, (E) Malic acid, (F) Succinic acid and (G) Glycine as precipitants.

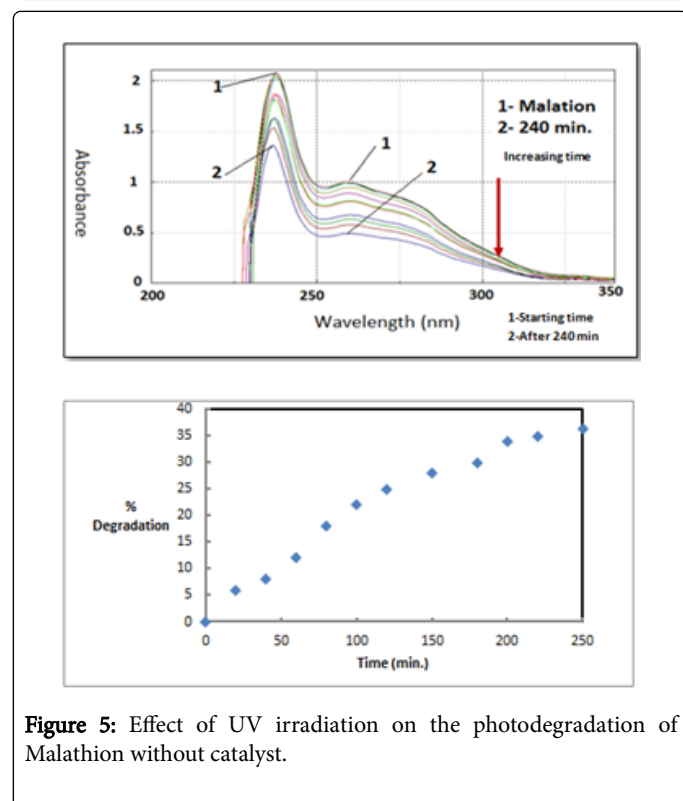


**Figure 5:** Effect of UV irradiation on the photodegradation of Malathion without catalyst.

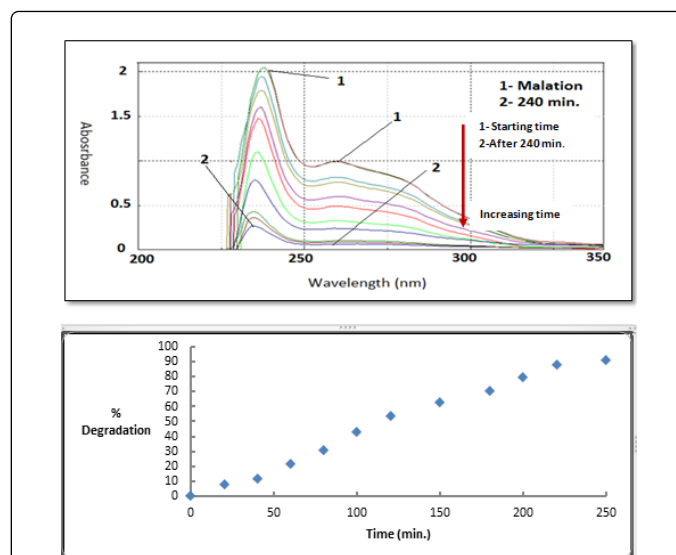
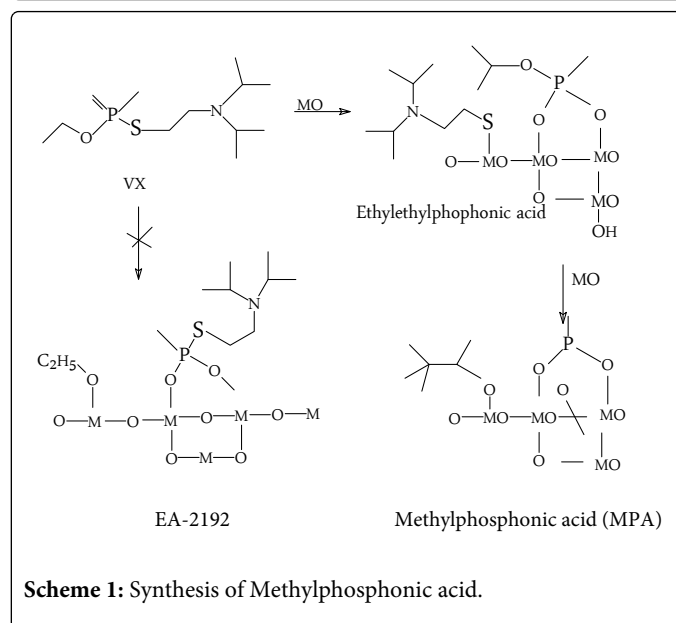


**Figure 6:** Effect of UV irradiation and sample MZ7 as catalyst on the photodegradation of Malathion.



**Scheme 1:** Synthesis of Methylphosphonic acid.

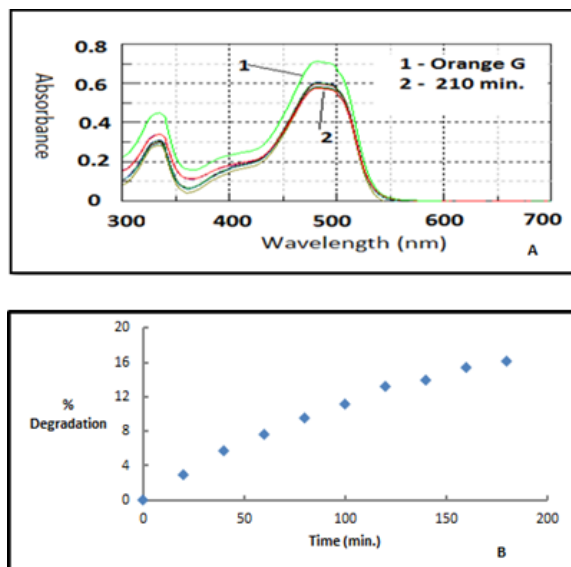


**Figure 7:** Effect of time on the (A) absorption spectra and (B) % degradation of OG under the influence of UV irradiation only.

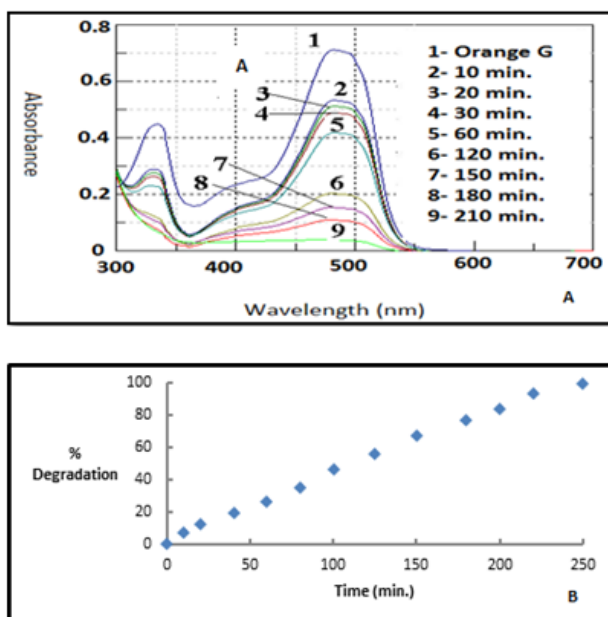


**Figure 8:** Effect of time on the (A) absorption spectra and (B) % degradation of OG under the influence of UV irradiation in presence of MZ1 as catalyst.

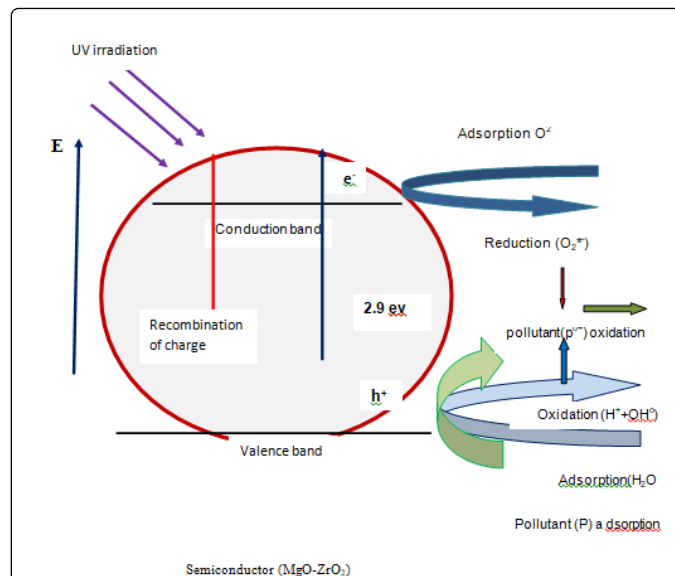


**Figure 9:** Principal of Mg-ZrO<sub>2</sub> photo catalyst.

## Conclusion

Different inexpensive organic acids and glycine were used as precursors for the preparation of mixed Mg-ZrO<sub>2</sub> nanoparticles (MZ1-MZ7) via co-precipitation-ignition route. The mixed Magnesium-Zirconium organic precursors and the corresponding nanooxides were characterized by thermal analysis and different spectroscopic techniques. The average crystal sizes of the nanocrystalline materials were found to depend on the starting organic precursors and lie within the range 10.79-47.55 nm with increasing order: Glycine<Tartaric acid<Oxalic acid<Malic acid<Citric acid<Malonic acid<Succinic acid. The optical energy gaps ( $E_g$ ) calculated from electronic absorption spectra ranged from 2.85-3.00 eV suggesting the semiconductor nature of the nanooxides. The products were tested as destructive adsorbents for Malathion as the stimulant of the CWA VX where it was found that complete decontamination took place within 240 min using MZ7 as sorbent. The photoactivity of the prepared samples was also assessed by the photocatalytic decomposition of OG dye in an aqueous solution under irradiation of UV radiation of 365 nm wavelength.

## Acknowledgment

We would like to acknowledge the financial support from the MSP (Management of Scientific Projects), Benha University, Benha, Egypt (project presented by I. M. Ibrahim).

## References

1. Neppolian B, Wang Q, Yamashita H, Choi H (2007) Synthesis and characterization of ZrO<sub>2</sub>-TiO<sub>2</sub> binary oxide semiconductor nanoparticles: application and interparticle electron transfer process. Appl Catal A Gen 333: 264-271.
2. Lara-García HA, Romero-Ibarra IC, Pfeiffer H (2014) Hierarchical N-doped cubic ZrO<sub>2</sub> synthesis by a simple hydrothermal route and its application in biodiesel production. J Solid State Chem 218: 213-220.
3. Zhao ZK, Ran JF (2015) Sulphated mesoporous La<sub>2</sub>O<sub>3</sub>-ZrO<sub>2</sub> composite oxide as an efficient and reusable solid acid catalyst for alkenylation of aromatics with phenylacetylene. Appl Catal A Gen 503: 77-83.

4. Soni KC, Shekar SC, Singh B, Gopi T (2015) Catalytic activity of Fe/ZrO<sub>2</sub> nanoparticles for dimethyl sulfide oxidation. J Colloid Interface Sci 446: 226-236.
5. Słońska A, Kaszewski J, Wolska-Kornio E, Witkowski B, Wachnicki Ł, et al. (2016) Luminescent properties of ZrO<sub>2</sub>: Tb nanoparticles for applications in neuroscience. Opt Mater 59: 96-102.
6. Atkinson I, Teoreanu I, Mocioiu OC, Smith ME, Zaharescu M (2010) Structure property relations in multicomponent oxide systems with additions of TiO<sub>2</sub> and ZrO<sub>2</sub> for glaze applications. J Non-Cryst Solids 356: 2437-2443.
7. Li S, Jiao Y, Wang Z, Jianli W, Quan Z, et al. (2015) Performance of RP-3 kerosene cracking over Pt/WO<sub>3</sub>-ZrO<sub>2</sub> catalyst. J Anal Appl Pyrolysis 113: 736-742.
8. Fakhri A, Behrouz S, Tyagi I, Agarwal S, Gupta VK (2016) Synthesis and characterization of ZrO<sub>2</sub> and carbon-doped ZrO<sub>2</sub> nanoparticles for photocatalytic application. J Mol Liq 216: 342-346.
9. Sherly ED, Vijaya JJ, Selvam NCS, Kennedy LJ (2014) Microwave assisted combustion synthesis of coupled ZnO-ZrO<sub>2</sub> nanoparticles and their role in the photocatalytic degradation of 2,4-dichlorophenol. Ceram Int 40: 5681-5691.
10. Qu X, Xie D, Cao L, Du F (2014) Synthesis and characterization of TiO<sub>2</sub>/ZrO<sub>2</sub> coaxial core-shell composite nanotubes for photocatalytic applications. Ceram Int 40: 12647-12653.
11. Bansal P, Chaudhary GR, Mehta SK (2015) Comparative study of catalytic activity of ZrO<sub>2</sub> nanoparticles for sonocatalytic and photocatalytic degradation of cationic and anionic dyes. Chem Eng J 280: 475-485.
12. Renuka L, Anantharaju KS, Sharma SC, Nagaswarupa HP, Prashantha SC, et al. (2016) Hollow microspheres Mg-doped ZrO<sub>2</sub> nanoparticles: green assisted synthesis and applications in photocatalysis and photoluminescence. J Alloys Compd 672: 609-622.
13. Columbus I, Waysbort D, Shmueli L, Nir I, Kaplan D (2006) Decomposition of adsorbed VX on activated carbons studied by 31P MAS NMR. Environ Sci Tech 40: 3952-3958.
14. Osovsky R, Kaplan D, Nir I, Rotter H, Elisha S, et al. (2014) Decontamination of adsorbed chemical warfare agents on activated carbon using hydrogen peroxide solutions. Environ Sci Technol 48: 10912-10918.
15. Kataoka K, Seto Y (2015) Measurement of breakthrough volumes of volatile chemical warfare agents on a poly(2,6-diphenylphenylene oxide)-based adsorbent and application to thermal desorption-gas chromatography/mass spectrometric analysis. J Chromatogr A 4: 1410-1419.
16. Marciano D, Goldvaser M, Columbus I, Zafrani Y (2011) Catalytic degradation of the nerve agent VX by water-swelled polystyrene-supported ammonium fluorides. J Org Chem 76: 8549-8553.
17. Chen W, Ran R, Weng D, Han S (2015) A facile ceria-zirconia binary oxide used for degradation of 2-chloroethyl ethyl sulfide. J Mater Sci 50: 6268-6276.
18. Sharma N, Kakkar R (2013) Recent advancements on warfare agents/metal oxides surface chemistry and their simulation study. Adv Mat Lett 4: 508-521.
19. Ashkarran AA, Afshar SAA, Aghigh SM, Mona K (2010) Photocatalytic activity of ZrO<sub>2</sub> nanoparticles prepared by electrical arc discharge method in water. Polyhedron 29: 1370-1374.
20. Ibrahim IM, Moustafa ME, Abdelhamid MR (2016) Effect of organic acid precursors on the morphology and size of ZrO<sub>2</sub> nanoparticles for photocatalytic degradation of Orange G dye from aqueous solutions. J Molec Liq 223: 741-748.
21. Dhre SL (2015) Silica-zirconia alkali-resistant coatings by sol-gel route. Curr Sci 108: 1647-1652.
22. Aly HM, Moustafa ME, Nassar MY, Abdelrahman EA (2015) Synthesis and characterization of novel Cu (II) complexes with 3-substituted-4-amino-5-mercapto-1,2,4-triazole Schiff bases: a new route to CuO nanoparticles. J Mol Struct 1086: 223-231.
23. Wagner GW, Bartram PW, Koper O, Klabunde KJ (1999) Reactions of VX, GD, and HD with Nanoscale MgO. J Phys Chem B 103: 3225-3228.
24. Sultana S, Rafiuddin M, Khan Z, Shahadat M (2015) Development of ZnO and ZrO<sub>2</sub> nanoparticles: Their photocatalytic and bactericidal activity. J Environ Chem Eng 3: 886-891.